



A novel dielectric barrier discharge reactor with photocatalytic electrode based on sintered metal fibers for abatement of xylene

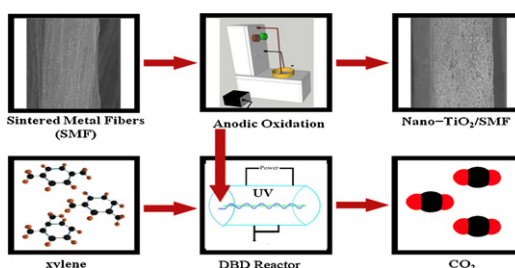
Zhiping Ye, Chunxia Wang, Zhenhua Shao, Qing Ye, Yi He, Yao Shi*

Key Laboratory of Biomass Chemical Engineering of Ministry of Education, Institute of Industrial Ecology and Environment, Department of Chemical and Biological Engineering, Zhejiang University (XiXi Campus), Hangzhou 310028, PR China

HIGHLIGHTS

- ▶ It is the different and convenient SMF catalyst preparation way.
- ▶ The combining of DBD and photocatalytic SMF electrode can effectively destroys xylene.
- ▶ It introduces the new combining way of DBD and SMF catalyst.

GRAPHICAL ABSTRACT



ARTICLE INFO

Article history:

Received 25 June 2012

Received in revised form 22 August 2012

Accepted 14 September 2012

Available online 21 September 2012

Keywords:

Nano-TiO₂/SMF electrode
Dielectric barrier discharge
Xylene
Anodic oxidation
Ti³⁺

ABSTRACT

A novel dielectric barrier discharge (DBD) reactor was made for the abatement of xylene. This reactor has a photocatalytic electrode prepared by a modified anodic oxidation method which was proposed in this work. The photocatalytic electrode has nano-TiO₂ deposited on sintered metal fiber (SMF). The reactor using the nano-TiO₂/SMF electrode shows much better performance in abating xylene compared with reactors using other electrodes such as resistance wire or SMF. The conversion ratio of xylene reaches 92.7% in the novel reactor at a relatively voltage (23.6 kV). This ratio is much higher than the conversion ratios of xylene in the traditional reactors with resistance wire or SMF electrodes, which are ~64.7%. The selectivity of CO₂ of the reactor using the nano-TiO₂/SMF electrode (300 pps, 23.6 kV) was observed to be 86.6%, which is about twice as large as that of a traditional reactor using a resistance wire electrode. If a traditional DBD reactor is replaced by the novel reactor, at the same specific input energy, the energy yield can increase from 0.391 to 0.556 mg/kJ. Finally, the xylene decomposition mechanism with the nano-TiO₂/SMF electrode was also briefly discussed.

© 2012 Elsevier B.V. All rights reserved.

1. Introduction

The atmospheric emissions of volatile organic compounds (VOCs) have been an increasing problem because of their detrimental effects on both human health and public environment. Among these VOCs, xylene has received more and more public attention [1]. Xylene is often used to replace toluene as an ingredient for paints and diluents. The inhalation of xylene can cause severe

gastrointestinal distress in humans. It can also lead to chemical pneumonitis, pulmonary edema, and hemorrhage [2].

Traditional xylene abatement methods, such as adsorption, biofiltration, photo catalytic degradation, have several disadvantages. For example, biofiltration can be easily affected by temperature or concentrations of pollutants [3]. Recently, applying non-thermal plasma (NTP) technology in VOCs control has attracted more and more attention because of its relatively low energy consumption and high removal efficiency. Dielectric barrier discharge (DBD) is one of the methods to generate NTP and has advantages over other types of discharge approaches due to the simplicity and scalability of its experimental setup [4].

* Corresponding author. Tel.: +86 571 88273591; fax: +86 571 88273693.
E-mail address: shiyao@zju.edu.cn (Y. Shi).

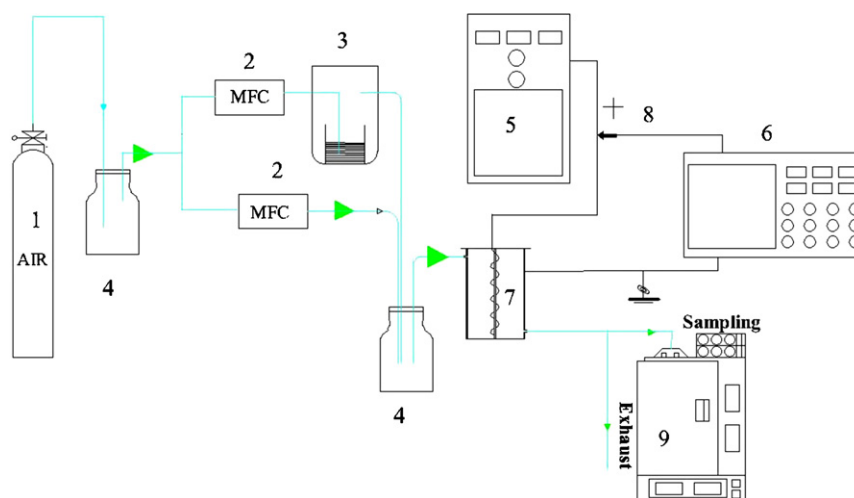


Fig. 1. Schematic diagram of the experimental setup ((1) air cylinder; (2) mass flow controllers (MFC); (3) bubbling; (4) buffer tank; (5) high voltage pulse source; (6) digital storage oscilloscope; (7) DBD reactor; (8) high voltage probe; (9) gas chromatograph).

The further development of DBD largely focuses on improving the energy efficiency for the effective removal of VOCs and the selectivity of CO_2 (the ratio of the carbon amount from effluent CO_2 to that from VOCs removed). Combined plasma catalyst reactors were shown to be effective for these purposes [5–9]. One way to make a combined plasma catalyst reactor is to use sintered metal fibers (SMF), on which a catalyst is placed. SMF is useful in a broad range of applications [10–13]. The high mechanical strength of SMF, as well as its chemical and thermal stability, makes it an ideal support for the catalyst [14]. SMF can help short-lived chemically active species generated in the plasma reach the catalyst surface in downstream configuration [15,16], therefore, the abatement performance of VOCs such as toluene, isopropanol, and trichloroethylene can be enhanced [17].

In order to effectively abate xylene, using nano- TiO_2 modified SMF electrodes seems to be a promising alternative approach. It will allow obtaining the synergy between plasma excitation and photocatalysis of TiO_2 on SMF electrodes. Ultraviolet (UV) light can activate photocatalyst due to the radioactive transitions of excited nitrogen [18,19]. Spyrou and Manassis observed that the typical emission spectrum of the discharge is in the range of 250–500 nm from excited species of nitrogen [20]. The energy of the emission is equivalent to the band gap of TiO_2 (3.2 eV) [21], which explains the mechanism of the catalytic process. Recently, Sumitsawan et al. reported that surface modified TiO_2 catalysts show improved photocatalytic oxidation capability for gaseous m-xylene [22], which further supports that idea of using nano- TiO_2 modified SMF electrodes to improve the abatement efficiency of xylene.

With traditional methods, it is complicate to load SMF electrodes with nano- TiO_2 . In this work, we employed a modified anodic oxidation method to prepare nano- TiO_2 /SMF electrodes [23,24]. Both the destruction ratio of xylene and the energy yield (EY) of nano- TiO_2 /SMF assisted DBD reactors were examined. The EY, the selectivity of CO_2 , and the demand factor for ozone (DF_{ozone}) were used to evaluate the efficiency of the abatement of xylene. The effects of applied voltage, pulse frequency, and the formation of ozone on the performance of this novel DBD reactor were also studied. In addition, scanning electron microscopy (SEM) and ultrasound adherence tests were performed for the characterization of the nano- TiO_2 /SMF.

2. Experimental details

2.1. Preparation of nano- TiO_2 /SMF electrode

The nano- TiO_2 /SMF electrode was made with a modified anodic oxidation method. First, SMF (Xi'an Filter Metal Materials Co. Ltd., China) was immersed in 10% H_2SO_4 solution for 5 min to dissolve the air-formed oxide film on the surface. SMF and a stainless steel wire (Hangzhou Fangcheng Metal Products Co. Ltd., China) were then connected to the anode and the cathode of a regulated DC power supply system (APS3003S, Atten Co. Ltd., China), respectively. The radius of anode and cathode are 0.022 mm and 0.35 mm, correspondingly. Both SMF and the stainless steel wire were immersed into 10% H_2SO_4 solution in a beaker. This step is for anodic oxidation of the SMF. The anodic oxidation lasted for 30 min at a current of 0.8 A. SMF was then rinsed with distilled water and dried in an oven at 373 K. SMF was further processed by impregnating in a mixture of 0.5 ml 10% anatase nano- TiO_2 solutions (VK-TG02, Wangjing Material Co. Ltd., China) and 50 ml distilled water. The mixture was stirred by heating magnetic stirrer until the liquid got evaporated in air at 373 K. Finally, nano- TiO_2 /SMF electrode was obtained after calcination at 773 K in air for 1.5 h. It contains 4 wt% of the metal oxide. The electrical resistance of the nano- TiO_2 /SMF electrode was measured to be $0.192 \pm 0.015 \Omega \text{ cm}$.

2.2. Characterization methods

X-ray photoelectron spectroscopy (XPS) experiments were performed on a VG scientific ESCA LAB MARK II (resolution 0.1 eV) with Mg K α radiation ($h\nu = 1253.6 \text{ eV}$). The X-ray gun ran at 250 W (10 kV, 25 mA) with a detection angle at 54° . To obtain sufficient resolution and sensitivity, the pass energy was fixed at 50 eV. Both the overview spectrum (0–1000 eV) and the narrow regions corresponding to Ti (450–470 eV) spectrum were recorded. The narrow spectrogram of Ti with higher resolution was recorded by using RBD 147 interface (RBD Enterprises, U.S.A.) with the Augerscan 3.21 software. For scans in narrow regions, the step size was 0.2 eV. The deconvolution of the main Ti 2p peak was done by CasaXPS software. After a Shirley background subtraction, the peaks were fitted by using a nonlinear, least squares subroutine with mixed Gauss–Lorentz functions.

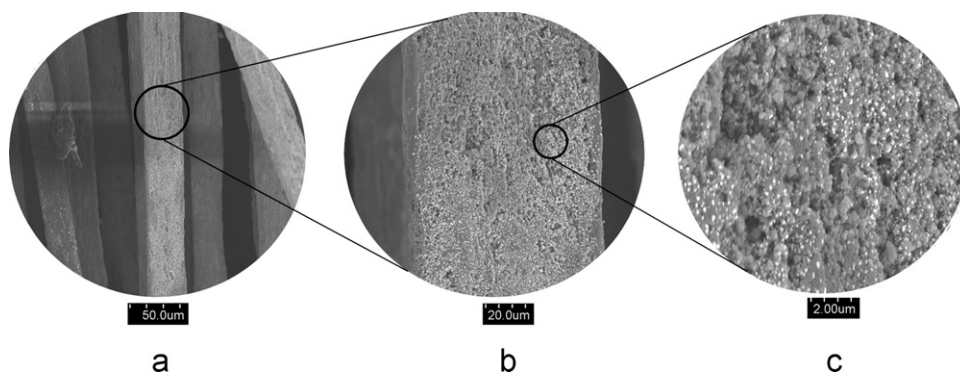


Fig. 2. Three-level SEM micrographs of nano-TiO₂/SMF: (a) nano-TiO₂/SMF at 1000 \times , (b) nano-TiO₂/SMF at 2000 \times , (c) nano-TiO₂/SMF at 20,000 \times .

The surface morphology of the nano-TiO₂/SMF electrode was examined by SEM (HITACHI S-4800). SEM micrographs at 1000 \times , 2000 \times and 20,000 \times were taken with an accelerating voltage of 3–5 kV. Before SEM analysis, the sample was put in an ultrasonic cleaner (Leijunda Ultrasonic Corp., China) containing ethanol and oscillated for 1 h to clean the surface [25]. The sample was then dried at 373 K and weighed.

2.3. Experimental setup and procedure

The experimental setup consists of a xylene feeding system, a DBD reactor, a high voltage pulse generator, and several other instruments (Fig. 1). Air from gas cylinders was allowed entering the xylene feeding system, where xylene was mixed with air in the buffer tank. The mixture was then fed into the plasma reactor. The concentration of xylene at the outlet was measured by the gas chromatograph equipped with a flame ionization detector (FID, GC7890II, Fuli Analytical Instrument Company, China). Hydrogen (pressure: 0.2 MPa) was the combustible gas, nitrogen (pressure: 0.5 MPa) was the carrier gas, and air was used to support the flame (pressure: 0.5 MPa), LOD (limit of detection): 1×10^{-11} g/s, temperature control accuracy: 0.1 $^{\circ}$ C; A ATSE-54 30 m \times 0.32 mm \times 0.5 μ m phenyl methyl silicone fused silica capillary column; detection temperature: 150 $^{\circ}$ C; oven temperature: 100 $^{\circ}$ C; auxiliary temperature: 150 $^{\circ}$ C. The standard curve of xylene in GC was used gas chromatography external standard method.

While ozone formed in the DBD reactor was measured with an UV absorption ozone monitor (API-450 NEMA). The formation of CO₂ was monitored with an infrared gas analyzer (Siemens Ultramat 22). The mixed stream was fixed at 800 ml/min at room temperature.

2.4. Plasma reactor, power supply and electrical measurements

The discharge was generated in a 70 mm (inner diameter) \times 150 mm polymethylmethacrylate (PMMA) cylinder with wall thickness of 5 mm and a cylindrical tube of 20 mm in diameter fixed along its axis, where the resistance wire (Yangzhou Tangchao Machinery Factory, China) and the SMF were wrapped round as inner electrode, while the SMF also served as the catalyst (Fig. S1). The stainless steel mesh was embedded between the discharge tube and the PMMA cylinder with a diameter of 90 mm, acting as the ground electrode. The discharge length was 150 mm and the discharge gap was around 20 mm referred to industrial application.

The detailed description of the Blumlein pulse forming network (BPFN) narrow pulse generator has been published elsewhere [26]. The peak voltage in the range of 16.6–23.6 kV was applied to different electrodes in a frequency varied from 100 to 300 pps (pulse per second). The conversion of xylene at each peak voltage

was measured every 30 min. The reproducibility of the results was checked and the error in all experimental measurements was less than $\pm 3.46\%$.

The voltage–charge (V – Q) Lissajous method was used to determine the discharge power in the DBD reactor. The electrical circuit was shown in Fig. S2. The charge Q was obtained from the voltage across a capacitor of 1 μ F connected in series to the ground electrode by voltage probe (Tektronix P6015A). The applied voltage was measured with a 1000:1 high voltage probe (Texas HVP-3020). The voltage and charge waveforms were recorded by a four channel digital oscilloscope (Tektronix, TDS 2014B) being capable of sampling 1GS/s (giga sample per second). With the voltage–charge (V – Q) Lissajous method, the voltage produced by DBD, and EY under different conditions can be measured. The explanation of EY was described in the supporting information.

3. Results and discussion

3.1. Characterization of nano-TiO₂/SMF electrode

The SEM images in Fig. 2 show that nano-TiO₂ has been successfully deposited onto the porous SMF surface. Compare with SMF surfaces without deposited nano-TiO₂ (Fig. S5), nano-TiO₂/SMF has higher surface roughness which increases the effective surface area for catalytic reactions. The change in surface roughness is a result of anodic oxidation in the H₂SO₄ solution [27]. During the anodic oxidation process, anions travel to the surfaces of SMF and react with metal ions on the SMF surface. The reaction not only leads to the generation of new pores but also enlarges some small pores which have already existed on SMF surface. These pores later become the hosts for nano-TiO₂.

The chemical composition of nano-TiO₂/SMF was measured by XPS. As shown Fig. 3, the Ti 2p_{3/2}, Ti 2p_{1/2}, Ti³⁺ 2p_{3/2} and Ti³⁺ 2p_{1/2} core levels were located at 458.5 \pm 0.02 eV, 464.2 \pm 0.02 eV, 457.0 \pm 0.04 eV and 462 \pm 0.04 eV, respectively [28,29].

The adherence of nano-TiO₂ has been evaluated by measuring the weight loss of the nano-TiO₂/SMF electrode caused by exposure to ultrasounds. The electrode was immersed in ethanol inside an ultrasound cleaner and treated in an ultrasound bath for 1 h. Table S1 shows that detachment ratio of the nano-TiO₂ was approximately 10% of the weights of nano-TiO₂/SMF electrodes. Meanwhile, XPS measurements of the nano-TiO₂/SMF electrodes (Fig. 4), made both before and after ultrasonic treatments, show a similar trend as what was observed in Table S1. Both ultrasound treatments and XPS results indicate a strong adherence of nano-TiO₂ on SMF with the modified anodic oxidation method.

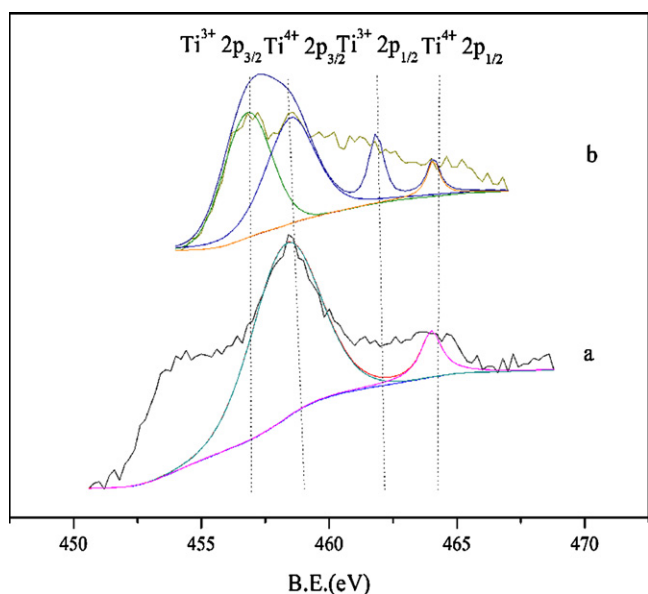


Fig. 3. Ti XPS spectra of the catalysts of (a) fresh nano-TiO₂/SMF and (b) aged nano-TiO₂/SMF after xylene decomposition reactions.

3.2. Effect of different electrodes on the conversion ratio of xylene

To evaluate the performance of the nano-TiO₂/SMF electrode, the conversion ratio of xylene by a regular SMF electrode and a resistance wire electrode were measured for comparison, respectively. For each electrode, its peak voltage was varied from 16.6 to 23.6 kV at a fixed pulse frequency of 300 pps. As shown in Fig. 5, the conversion ratio of xylene increased with the increase of peak voltage of each electrode. These results can be explained with the change in the amount of active species generated by the electrodes. The higher peak voltages provide larger energy inputs and lead to greater amount of active species. These active species play a key role in the decomposition of xylene. Therefore, the conversion ratio of xylene is enhanced. Similar effect was also found in the decomposition of polluting gases in other studies [5]. Fig. 5 also shows that the abatement of xylene with the nano-TiO₂/SMF electrode was much more effective than the other two electrodes. The

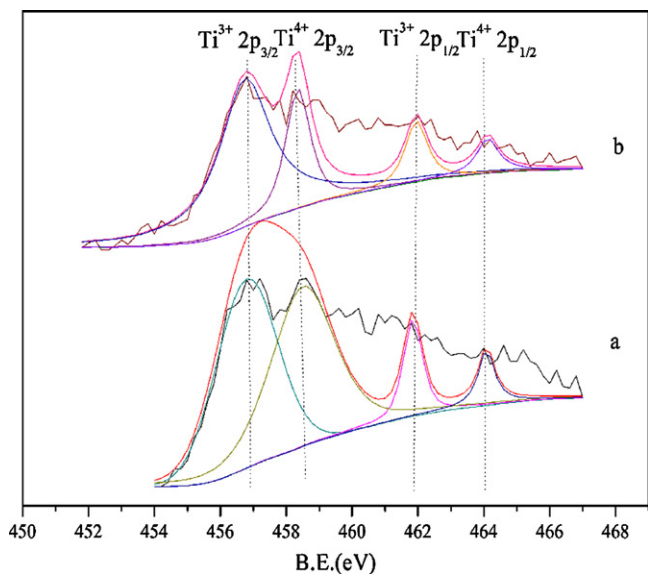


Fig. 4. Ti XPS spectra of the catalyst of (a) SMF catalyst electrode before ultrasonic vibration and (b) SMF catalyst electrode after ultrasonic vibration.

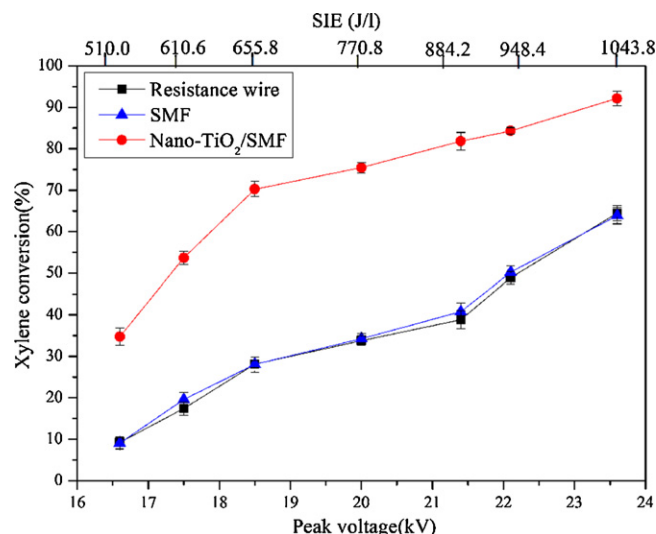


Fig. 5. Effect of the peak voltage on the destruction of xylene over different electrodes (initial concentration: 431.8 ± 5 mg/m³; pulse frequency: 300 pps).

nano-TiO₂/SMF electrode can achieve a xylene conversion ratio as high as 92.7% at a peak voltage of 23.6 kV, while the SMF electrode and the resistance wire electrode, can only obtain a xylene conversion ratio of 64.8% and 64.7%, respectively at the same peak voltage. The removal ratio of xylene was improved sharply because of the activated nano-TiO₂/SMF. The irradiated nano-TiO₂/SMF has higher energy content than the band-gap. It produces electron-hole pairs which lead to redox reactions between separated electron-hole pairs and trapped VOCs [30,31].

Fig. 6 showed the selectivity to CO₂ as a function of the peak voltage at 300 pps for the nano-TiO₂/SMF and resistance wire electrodes, respectively. Most xylene is converted to CO₂ with the nano-TiO₂/SMF electrode. The decomposition performance of the nano-TiO₂/SMF electrode is much better than the resistance wire one, especially at high peak voltages. More CO₂ was formed with the decomposition of xylene when using the nano-TiO₂/SMF electrode. The selectivity of CO₂ increased from 44.3% to 86.6% with the increasing peak voltage for the nano-TiO₂/SMF electrode, whereas for the resistance wire electrode, the selectivity of CO₂ was only

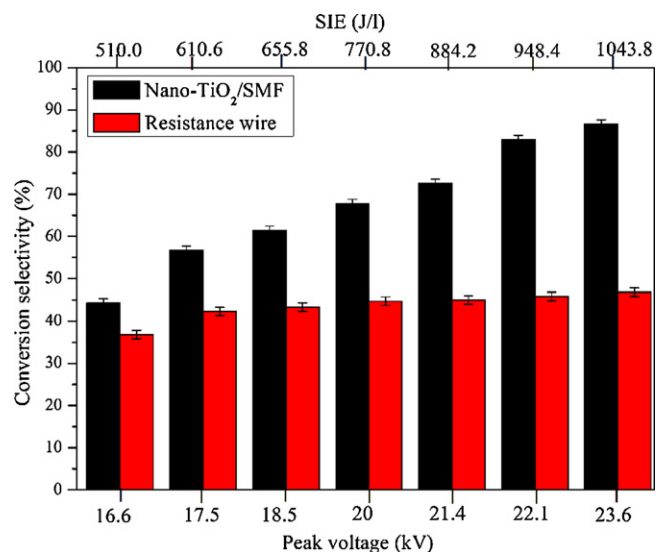


Fig. 6. Effect of the peak voltage on the selectivity to CO₂ (initial concentration: 431.8 ± 5 mg/m³; pulse frequency: 300 pps).

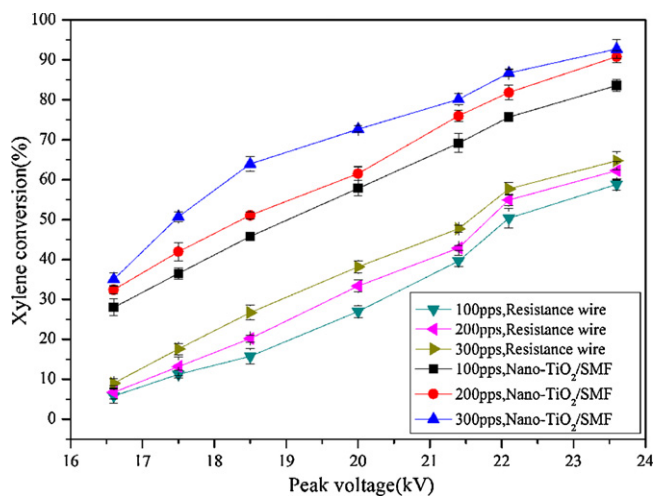


Fig. 7. Variation of the xylene conversion as a function of peak voltage and frequency using different electrodes (initial concentration: $431.8 \pm 5 \text{ mg/m}^3$).

about 46.8% and almost independent of the peak voltage in this study.

3.3. Effect of pulse frequency on decomposition of xylene

The effective removal of xylene relies on the synergy between nano-TiO₂/SMF and plasma produced by the DBD reactor. As the nature of plasma is closely related to the pulse frequency, it is important to examine the effect of the pulse frequency on the decomposition of xylene. As seen from Fig. 7, the destruction of xylene increased with the voltage (16.6–23.6 kV). When using the nano-TiO₂/SMF electrode, the conversion of xylene was improved at a constant frequency. The removal efficiency of xylene at 23.6 kV increased to 83.5%, 90.8% and 92.7%, versus 58.8%, 62.2% and 64.7% without the nano-TiO₂/SMF electrode from 100 pps to 300 pps. The effect of pulse frequency is closely related to the DBD discharge electrical properties: electric wind velocity, electrical power [32]. Forte found that the maximum velocity increased asymptotically with the applied voltage. The same result was observed with an increase in frequency [33]. The higher velocity is, the shorter reaction time is needed. As the DBD reactor can produce many short-lived active atoms and molecules, it will help the decomposition of xylene by using these active materials. At the same time, as the frequency increases, the discharge power input becomes greater [34]. The result indicated that the influence of pulse frequency on the removal efficiency of xylene was relatively small whether using a nano-TiO₂/SMF electrode or not.

Fig. 8 presented that the increase in the frequency and peak voltage can enhance the selectivity of CO₂. Using the nano-TiO₂/SMF electrode, the maximum selectivity of CO₂ was approximately 81.4% at 23.6 kV when the peak voltage was in a range of 16.6–23.6 kV (i.e. frequency 200 pps). When the frequency was increased to 300 pps, a CO₂ selectivity of ~86.6% was achieved at 23.6 kV. The undesired products were minimized at each frequency with the help of nano-TiO₂/SMF electrode. The CO₂ selectivity of resistance electrode was shown in Fig. S4 in the supporting information for comparison. The higher the frequency and the peak voltage were, the more the energy input was required, which helped produced higher energy and more activated species. These activated species can immediately react with xylene, or helped the nano-TiO₂/SMF be activated. The desired xylene oxidation to CO₂ was achieved by the selectivity of nano-TiO₂/SMF catalyst. However, operating the reactor at the highest CO₂ selectivity (300 pps, 23.6 kV) was not economically feasible, which will be further

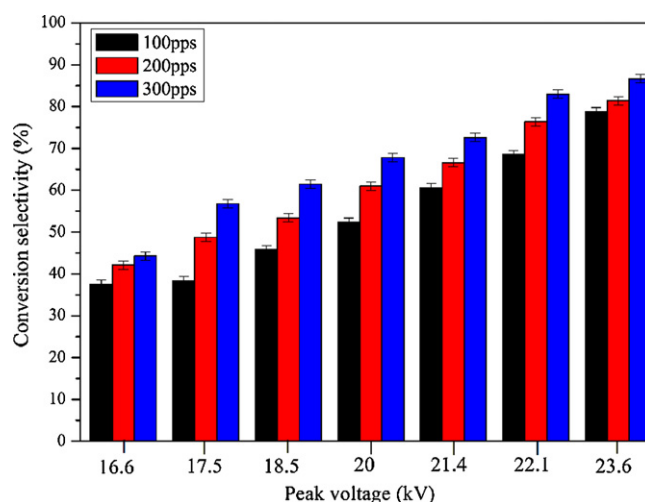


Fig. 8. Variation of the CO₂ selectivity as a function of frequency using nano-TiO₂/SMF electrode (initial concentration: $431.8 \pm 5 \text{ mg/m}^3$).

discussed in the following section. The result also suggested that the pulse frequency has insignificantly effects on the selectivity of CO₂ in a traditional DBD reactor. More undesirable products can be converted to CO₂ with the DBD reactor using the nano-TiO₂/SMF electrode.

3.4. Energy yield

Energy yield is one of the most important benchmarks for the evaluation of the performance of the DBD reactor. It can be used to estimate the economical feasibility of the reactor for industrial application [35]. As shown in Fig. S3, the specific input energy (SIE) was proportional to the frequency. It can explain that the effect of the pulse frequency on the degradation efficiency of xylene. It also suggested that destruction of xylene disproportionate change with the SIE.

In order to know if the reactor was energetically feasible for the conversion, Table 1 was obtained, which showed that the nano-TiO₂/SMF electrode had the better EY performance in the range of 100 to 300 pps. Table 1 also showed that even though the removal ratio of xylene was the lowest among the three frequencies (23.6 kV and 100 pps frequency), the corresponding EY (0.556 mg/kJ) was the highest one among the frequencies. It seems that the pulse frequency can improve the removal ratio of xylene and the selectivity of CO₂ because of the SIE, when the optimized reaction condition in air at room temperature was at 100 pps.

3.5. Formation of ozone

The formation of ozone is closely related to the performance of the DBD reactor with the nano-TiO₂/SMF electrode. Fig. 9 showed that before xylene treatment, the formation of ozone was 366.2 mg/m³ with the nano-TiO₂/SMF electrode, while the formation of ozone was 205.7 mg/m³ with the resistance wire electrode (300 pps). At the same time, when xylene went through the reactor, ozone production decreased with the increase of peak voltage. The concentration of ozone with the nano-TiO₂/SMF electrode was higher than that with the resistance wire electrode. It implied that the nano-TiO₂/SMF electrode was activated in the DBD. The effect of the UV light could be expected only if DBD emitted radiation, because emission from excited nitrogen molecules (N₂^{*}) was in the range of the band gap of the nano-TiO₂/SMF [19]. It explains why the high concentration of the ozone was formed. As the long-lived active species, the ozone helped decomposition of the xylene.

Table 1Comparison of energy yield at 100 pps, 200 pps, 300 pps (23.6 kV, initial concentration, $431.8 \pm 5 \text{ mg/m}^3$).

	100 pps		200 pps		300 pps	
	Resistance electrode	Nano-TiO ₂ /SMF electrode	Resistance electrode	Nano-TiO ₂ /SMF electrode	Resistance electrode	Nano-TiO ₂ /SMF electrode
Energy yield (mg/kJ)	0.391	0.556	0.303	0.442	0.268	0.384

In agreement with the finding, it had been reported that long-lived active oxygen species and ozone play an important role in a pulse corona reactor for benzene decomposition [36,37]. Some researchers suggested that on the ozone-assisted catalytic oxidation, the ozone decomposition on active sites may be expressed as follows [38]:



where * represents active sites.

Eqs. (1) and (2) suggested one of probably ways for xylene decomposition with the help of the ozone. In this system, the DBD could provide many active atoms and molecules, ionized atoms and molecules, electrons and so on. Some high energy species combined with the ozone promoted xylene destruction. From Fig. 6, it was easy to know that with the nano-TiO₂/SMF electrode, the ozone concentration was improved sharply. It was available for synergistic action.

Fig. 10 shows the consumption of the ozone at different electrodes in the presence of xylene. On the one hand, the ozone took part in the xylene decomposition. Ozone was one of the factors for high removal ratio because only a small part of the ozone was consumed. On the other hand, the consumption efficiency of O₃ should be taken into consideration. DF_{ozone} defined in supporting information was used to evaluate the system.

The information obtained from Fig. 11 was that, first of all, the lower DF_{ozone} was desirable for ozone-assisted catalytic oxidation in the perspective of energy efficiency. The ozone utilization ratio of the nano-TiO₂/SMF electrode was higher than resistance wire electrode at any peak voltage. Secondly, the interesting thing was that the highest ozone utilization ratio was achieved at 16.6 kV with the nano-TiO₂/SMF electrode, and the DF_{ozone} was 0.09155. However, the highest DF_{ozone} of resistance electrode was 0.6113

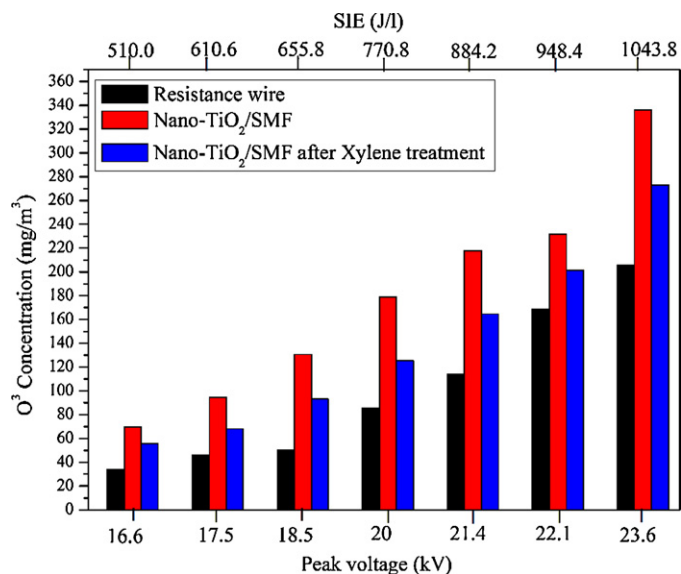


Fig. 9. The amount of ozone produced under different circumstances (300 pps, initial concentration: $431.8 \pm 5 \text{ mg/m}^3$).

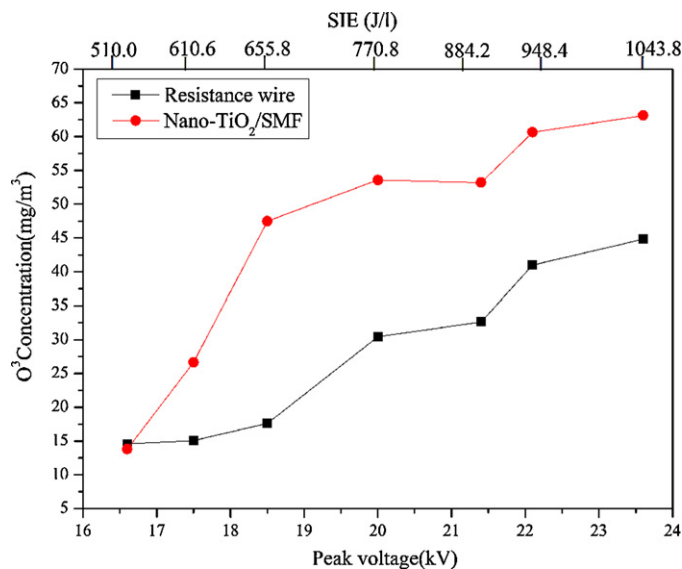


Fig. 10. Consumed ozone concentration as a function of catalyst in the presence of xylene (with resistance wire xylene initial concentration: $429.2 \pm 5 \text{ mg/m}^3$; with nano-TiO₂/SMF xylene initial concentration: $431.8 \pm 5 \text{ mg/m}^3$).

at the same peak voltage. Meanwhile, these results suggest that the system took full advantage of the ozone for the enhancement of xylene decomposition and the improvement of CO₂ selectivity. The ozone utilization ratio decreased with the increase of the peak voltage, though the removal ratio of xylene was improved when the peak voltage increased. The similar trend was found in different conditions.

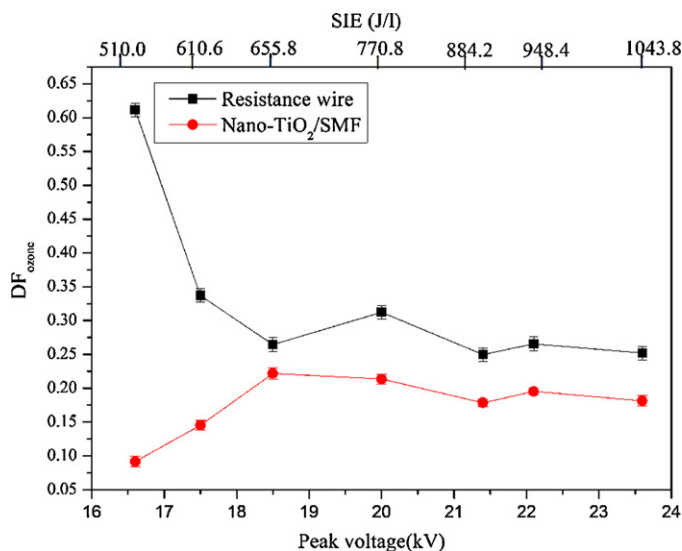


Fig. 11. Relationship between DF_{ozone} and peak voltage (300 pps, resistance wire initial concentration, $429.2 \pm 5 \text{ mg/m}^3$, nano-TiO₂/SMF initial concentration, $431.8 \pm 5 \text{ mg/m}^3$).

3.6. XPS analysis

In order to further investigate xylene decomposition mechanism of the novel DBD process, the result of XPS was analyzed. As seen from Fig. 3, it was certain that nano-TiO₂ was loaded on the SMF by modified anodic oxidation method described above. The presence of Ti³⁺ in XPS results suggests that there are some changes in the structure of the nano-TiO₂ to satisfy the requirement of overall charge balance. As many Ti³⁺ ions substitute for Ti⁴⁺, oxygen vacancies seems to what are produced to balance the charge.

Ti³⁺ ions have been suggested as mediators of photooxidation and photoreduction on TiO₂ [39]. In agreement with these findings, Szczepankiewicz et al. reported that the result was determined by the competition of the surface reaction of nano-TiO₂. Meanwhile, the competition also reflected the redox efficiency of the nano-TiO₂ [40].

Justicia et al. [41] found that the width of the TiO₂ forbidden band was related to the concentrations of Ti³⁺ ions or oxygen vacancies. By using electron paramagnetic resonance (EPR) spectra and the UV–vis spectra, Zuo et al. reached the conclusion that the Ti³⁺ inside the bulk TiO₂ was responsible for the band gap narrowing [42], which explains why the nano-TiO₂/SMF electrode has significantly enhanced performance in the photocatalysis process.

4. Conclusions

The DBD reactor with a photocatalytic SMF inner electrode was shown to be able to effectively decompose xylene and achieve a high selectivity of CO₂. The nano-TiO₂/SMF electrode was prepared with a modified anodic oxidization method which can successfully deposit nano-TiO₂ on SMF surfaces with strong adherence. The conversion ratio of xylene with this novel DBD reactor was improved significantly, even at relatively low voltage (23.6 kV). Under the same specific input energy, EY can be increased from 0.391 to 0.556 mg/kJ if the traditional DBD reactor was replaced by the novel DBD reactor with a nano-TiO₂/SMF electrode.

Acknowledgements

We gratefully acknowledge the financial support of Forestry Industry Research Special Funds for public welfare projects (No. 201204703) and the Scientific and Technological Innovation Team Foundation of Zhejiang Province (Grant No. 2009R50048).

Appendix A. Supplementary data

Supplementary data associated with this article can be found, in the online version, at <http://dx.doi.org/10.1016/j.jhazmat.2012.09.033>.

References

- [1] Y.J. Wang, Y. Zhang, L. Su, X.Y. Li, L. Duan, C.W. Wang, T.Y. Huang, Hazardous air pollutant formation from pyrolysis of typical Chinese casting materials, *Environ. Sci. Technol.* 45 (2011) 6539–6544.
- [2] A.F. Rosmarie, Toxicity Summary For Xylene, Managed by Martin Marietta Energy Systems, Inc., for the U.S. Department of Energy under Contract No. DE-AC05-84OR21400, Oak Ridge, TN, 1994.
- [3] H. Jorio, L. Bibeau, G. Viel, M. Heitz, Effects of gas flow rate and inlet concentration on xylene vapors biofiltration performance, *Chem. Eng. J.* 76 (2000) 209–221.
- [4] U. Kogelschatz, Dielectric-barrier discharges: their history, discharge physics, and industrial applications, *Plasma Chem. Plasma Process.* 23 (2003) 1–46.
- [5] J. Van Durme, J. Dewulf, C. Leys, H. Van Langenhove, Combining non-thermal plasma with heterogeneous catalysis in waste gas treatment: a review, *Appl. Catal. B: Environ.* 78 (2008) 324–333.
- [6] H.H. Kim, S.M. Oh, A. Ogata, S. Futamura, Decomposition of gas-phase benzene using plasma-driven catalyst (PDC) reactor packed with Ag/TiO₂ catalyst, *Appl. Catal. B: Environ.* 56 (2005) 213–220.
- [7] A.M. Vandembroucke, R. Morent, N. De Geyter, C. Leys, Non-thermal plasmas for non-catalytic and catalytic VOC abatement, *J. Hazard. Mater.* 195 (2011) 30–54.
- [8] U. Roland, F. Holzer, F.D. Kopinke, Combination of non-thermal plasma and heterogeneous catalysis for oxidation of volatile organic compounds, *Appl. Catal. B: Environ.* 58 (2005) 217–226.
- [9] U. Roland, F. Holzer, A. Poppl, F.D. Kopinke, Combination of non-thermal plasma and heterogeneous catalysis for oxidation of volatile organic compounds: Part 3. Electron paramagnetic resonance (EPR) studies of plasma-treated porous alumina, *Appl. Catal. B: Environ.* 58 (2005) 227–234.
- [10] J. Karupiah, R. Karvembu, C. Subrahmanyam, The catalytic effect of MnO_x and CoO_x on the decomposition of nitrobenzene in a non-thermal plasma reactor, *Chem. Eng. J.* 180 (2012) 39–45.
- [11] M. Crespo-Quesada, M. Grasmann, N. Semagina, A. Renken, L. Kiwi-Minsker, Kinetics of the solvent-free hydrogenation of 2-methyl-3-butyn-2-ol over a structured Pd-based catalyst, *Catal. Today* 147 (2009) 247–254.
- [12] A.M. Vandembroucke, R. Morent, N. De Geyter, C. Leys, Decomposition of trichloroethylene with plasma-catalysis: a review, *J. Adv. Oxid. Technol.* 14 (2011) 165–173.
- [13] C. Subrahmanyam, A. Renken, L. Kiwi-Minsker, Novel catalytic non-thermal plasma reactor for the abatement of VOCs, *Chem. Eng. J.* 134 (2007) 78–83.
- [14] I. Yuranov, A. Renken, L. Kiwi-Minsker, Zeolite/sintered metal fibers composites as effective structured catalysts, *Appl. Catal. A: Gen.* 281 (2005) 55–60.
- [15] H.L. Chen, H.M. Lee, S.H. Chen, M.B. Chang, S.J. Yu, S.N. Li, Removal of volatile organic compounds by single-stage and two-stage plasma catalysis systems: a review of the performance enhancement mechanisms, current status, and suitable applications, *Environ. Sci. Technol.* 43 (2009) 2216–2227.
- [16] C. Subrahmanyam, A. Renken, L. Kiwi-Minsker, Catalytic abatement of volatile organic compounds assisted by non-thermal plasma. Part II. Optimized catalytic electrode and operating conditions, *Appl. Catal. B: Environ.* 65 (2006) 157–162.
- [17] M. Magureanu, N.B. Mandache, V.I. Parvulescu, C. Subrahmanyam, A. Renken, L. Kiwi-Minsker, Improved performance of non-thermal plasma reactor during decomposition of trichloroethylene: optimization of the reactor geometry and introduction of catalytic electrode, *Appl. Catal. B: Environ.* 74 (2007) 270–277.
- [18] B.-Y. Lee, S.-H. Park, S.-C. Lee, M. Kang, S.-J. Choung, Decomposition of benzene by using a discharge plasma-photocatalyst hybrid system, *Catal. Today* 93–95 (2004) 769–776.
- [19] C. Subrahmanyam, M. Magureanu, D. Laub, A. Renken, L. Kiwi-Minsker, Non-thermal plasma abatement of trichloroethylene enhanced by photocatalysis, *J. Phys. Chem. C* 111 (2007) 4315–4318.
- [20] N. Spyrou, C. Manassis, Spectroscopic study of a positive streamer in a point-to-plane discharge in air – evaluation of the electric-field distribution, *J. Phys. D: Appl. Phys.* 22 (1989) 120–128.
- [21] X. Chen, S.S. Mao, Titanium dioxide nanomaterials: synthesis, properties, modifications, and applications, *Chem. Rev.* 107 (2007) 2891–2959.
- [22] S. Sumitsawan, J. Cho, M.L. Sattler, R.B. Timmons, Plasma surface modified TiO₂ nanoparticles: improved photocatalytic oxidation of gaseous m-xylene, *Environ. Sci. Technol.* 45 (2011) 6970–6977.
- [23] B. Yang, Preparation of bioactive titanium metal via anodic oxidation treatment, *Biomaterials* 25 (2004) 1003–1010.
- [24] J.E. Samad, J.A. Nychka, N.V. Semagina, Structured catalysts via multiple stage thermal oxidation synthesis of FeCrAl alloy sintered microfibers, *Chem. Eng. J.* 168 (2011) 470–476.
- [25] M. Valentini, G. Groppi, C. Cristiani, M. Levi, E. Tronconi, P. Forzatti, The deposition of gamma-Al₂O₃ layers on ceramic and metallic supports for the preparation of structured catalysts, *Catal. Today* 69 (2001) 307–314.
- [26] J. Chen, J.T. Yang, H. Pan, Q.F. Su, Y.M. Liu, Y. Shi, Abatement of malodorants from pesticide factory in dielectric barrier discharges, *J. Hazard. Mater.* 177 (2010) 908–913.
- [27] M.V. Diamanti, M.P. Pedferri, Effect of anodic oxidation parameters on the titanium oxides formation, *Corros. Sci.* 49 (2007) 939–948.
- [28] R. Sanjines, H. Tang, H. Berger, F. Gozzo, G. Margaritondo, F. Levy, Electronic-structure of anatase TiO₂ oxide, *J. Appl. Phys.* 75 (1994) 2945–2951.
- [29] S. Sodergren, H. Siegbahn, H. Rensmo, H. Lindstrom, A. Hagfeldt, S.E. Lindquist, Lithium intercalation in nanoporous anatase TiO₂ studied with XPS, *J. Phys. Chem. B* 101 (1997) 3087–3090.
- [30] K. Demeestere, J. Dewulf, T. Ohno, P.H. Salgado, H. Van Langenhove, Visible light mediated photocatalytic degradation of gaseous trichloroethylene and dimethyl sulfide on modified titanium dioxide, *Appl. Catal. B: Environ.* 61 (2005) 140–149.
- [31] A.L. Linsebigler, G.Q. Lu, J.T. Yates, Photocatalysis on TiO₂ surfaces – principles, mechanisms, and selected results, *Chem. Rev.* 95 (1995) 735–758.
- [32] E. Moreau, Airflow control by non-thermal plasma actuators, *J. Phys. D: Appl. Phys.* 40 (2007) 605–636.
- [33] M. Forte, J. Jolibois, J. Pons, E. Moreau, G. Touchard, M. Cazalens, Optimization of a dielectric barrier discharge actuator by stationary and non-stationary measurements of the induced flow velocity: application to airflow control, *Exp. Fluids* 43 (2007) 917–928.
- [34] J. Pons, E. Moreau, G. Touchard, Asymmetric surface dielectric barrier discharge in air at atmospheric pressure: electrical properties and induced airflow characteristics, *J. Phys. D: Appl. Phys.* 38 (2005) 3635–3642.

- [35] H.H. Kim, G. Prieto, K. Takashima, S. Katsura, A. Mizuno, Performance evaluation of discharge plasma process for gaseous pollutant removal, *J. Electrostat.* 55 (2002) 25–41.
- [36] J. Chen, Q.F. Su, H. Pan, J.W. Wei, X.M. Zhang, Y. Shi, Influence of balance gas mixture on decomposition of dimethyl sulfide in a wire-cylinder pulse corona reactor, *Chemosphere* 75 (2009) 261–265.
- [37] A. Ogata, N. Shintani, K. Mizuno, S. Kushiya, T. Yamamoto, Decomposition of benzene using a nonthermal plasma reactor packed with ferroelectric pellets, *IEEE Trans. Ind. Appl.* 35 (1999) 753–759.
- [38] M. Sugawara, A. Ogata, Effect of different combinations of metal and zeolite on ozone-assisted catalysis for toluene removal, *Ozone: Sci. Eng.* 33 (2011) 158–163.
- [39] H. Idriss, E.G. Seebauer, Photooxidation of ethanol on Fe–Ti oxide particulates, *Langmuir* 14 (1998) 6146–6150.
- [40] S.H. Szczepankiewicz, A.J. Colussi, M.R. Hoffmann, Infrared spectra of photoinduced species on hydroxylated titania surfaces, *J. Phys. Chem. B* 104 (2000) 9842–9850.
- [41] I. Justicia, P. Ordejon, G. Canto, J.L. Mozos, J. Fraxedas, G.A. Battiston, R. Gerbasi, A. Figueras, Designed self-doped titanium oxide thin films for efficient visible-light photocatalysis, *Adv. Mater.* 14 (2002) 1399–1402.
- [42] F. Zuo, L. Wang, T. Wu, Z.Y. Zhang, D. Borchardt, P.Y. Feng, Self-doped Ti^{3+} enhanced photocatalyst for hydrogen production under visible light, *J. Am. Chem. Soc.* 132 (2010) 11856–11857.